PNAS
www.pnas.org

# Supplementary Information for

## Doping evolution of the Mott-Hubbard landscape in infinite-layer nickelates

**Berit H. Goodge, Danfeng Li, Kyuho Lee, Motoki Osada, Bai Yang Wang, George A. Sawatzky, Harold Y. Hwang, & Lena F. Kourkoutis**

**Lena F. Kourkoutis**
**E-mail: lena.f.kourkoutis@cornell.edu**

**This PDF file includes:**





www.pnas.org/cgi/doi/10.1073/pnas.2007683118

## Supporting Information Text

### Local sample variations

Spatially localized spectroscopic measurements are crucial to limit contributions not only from the $SrTiO_3$ substrate and capping layer but also from crystallographic defects and secondary structural phases. Epitaxial growth with non-optimized growth conditions can result in precursor growth phases in the Ruddlesden-Popper (RP) series $(Nd,Sr)_{n+1}Ni_nO_{3n+1}$ through the formation of excess NdO planes in the perovskite film, as described in (1). Topotactic reduction of these phases form in turn $(Nd,Sr)_{n+1}Ni_nO_{2n+2}$ reduced films. X-ray diffraction (XRD) $\theta$-$2\theta$ measurements of such films suggest a close lattice match to the $n = 3$ RP phases in both the as-grown and reduced films. The HAADF-STEM imaging shown in Fig. S1 confirms a high density of vertical NdO plane faults consistent with this approximation. Importantly for spectroscopic characterization of these films, these secondary phases exhibit markedly different electronic structures in the O-K EELS edge as compared to $NdNiO_3$ and $NdNiO_2$. Representative O-K EEL spectra from the films are shown in Fig. S1c along with spectra from the corresponding pure perovskite and infinite-layer phases. The most prominent difference between each optimized/secondary phase pair ($(Nd,Sr)NiO_3$/$(Nd,Sr)_4Ni_3O_{10}$ and $(Nd,Sr)NiO_2$/$(Nd,Sr)_4Ni_3O_8$) is an extra peak at ~530 eV that appears in each of the secondary phases, attributed to the additional RP planes. Importantly, in the reduced films, this feature forms an extra shoulder within ~2 eV of the observed doping-dependent feature discussed in the main text Fig. 4. We also note that while the early films shown in Fig. S1 appear to be dominated by these secondary phase structures, even the more fully optimized films have local regions which exhibit RP faults. It is therefore important to isolate spectroscopic measurements away from regions where this RP signature could hamper the analysis of the doping peak.

In the same way that the epitaxial growth process can form local regions of non-optimized crystalline structure, the chemical topotactic reduction process to the infinite-layer phase can result in similar degrees of non-uniformity throughout the films, namely as local pockets of partial oxygen reduction to $NdNiO_{2+\delta}$. Previous experiments and structural refinements have also suggested inhomogeneous reduction of the perovskite phase in bulk compounds of both La and Nd nickelates (3, 4). While secondary RP phases and extended crystalline defects can in general be identified and avoided based on the lattice structure observed in HAADF-STEM, variations in O content, however, are essentially indistinguishable without spectroscopic measurements. Figure S2a,b show regions of what appear to be relatively clean crystallographic growth in a nominally reduced $NdNiO_2$ film. A number of O-K spectra from throughout the same film (Fig. S2c), however, show incomplete suppression of the $d^9$ pre-peak at 527 eV, suggesting incomplete reduction to $NdNiO_2$. For the results presented here, we therefore not only localize our spectroscopic measurements to avoid crystalline defects, but also to avoid regions of O off-stoichiometry. In order to exclude contributions from any such O-rich regions, any spectra with O-K edge onset before 527 eV were discounted from further analysis. Furthermore, only regions which show full reduction to $Nd_{1-x}Sr_xNiO_2$ in the O-K edge were considered for analysis of the Ni and Nd edges, ensuring that measurements of all three contributions can be ascribed to the pure infinite-layer phase.

### Nd-$M_{4,5}$ EELS edge across the nickelate series

The $4f$ states of Nd are probed via the Nd-$M_{4,5}$ core-loss edges at 978 and 1000 eV as shown in Fig. S4. All films studied in this series showed identical Nd-$M_{4,5}$ edge fine structure consistent with the expected $Nd^{3+}$ formal valence (6), independent of O stoichiometry or hole doping. The Nd-$M_{4,5}$ edge is therefore also useful as a reliable reference point for the absolute energy alignment of other spectra, most notably the Ni-$L_{2,3}$ edge, in order to reveal subtle spectroscopic differences between samples.

### Consideration of radiation damage

The effects of electron beam-induced radiation damage must be considered to ensure the fidelity of our measurements. All EELS experiments presented here were conducted with a ~1 Å probe, a scan pixel size of ~0.1 $Å^2$ and a dwell time of 0.5 $\mu$s/pixel. For the sake of simplicity we therefore discuss the corresponding electron dose rate in terms of probe current, which can in turn be converted to electron dose rates of $e^-/Å^2/s$. At 100 kV, a beam current of 27 pA was found to induce significant modification to the O-K edge of an unreduced $NdNiO_3$ film, as shown in Fig. S7. Interestingly, the progression of this edge as a function of total exposed dose suggests that the primary effect of the electron beam is to reduce O in the film, pushing it towards $NdNiO_2$ character. In contrast, the $NdNiO_2$ films begins to undergo more significant changes evidenced by the growth of a peak at ~532 eV. After exposure to very extreme doses (~2 nA beam current), structural changes can be observed in HAADF-STEM, suggesting transformation to a Ni-rich phase. Using the scan conditions listed above, repeated experiments in several films (both reduced and unreduced) showed no electronic modification in any sample at beam currents of ~20 pA, which was subsequently set as the damage-limited threshold. For EELS acquisitions, we lowered the current to ~9-12 pA – well below this threshold – and observed no modification in the O-K edge even for very long total exposure times (~2000 seconds or more). For a given region, the O-K edge was checked before each measurement to confirm the expected O stoichiometry (as discussed above) and again after all measurements to ensure no electronic modification had taken place under the beam.

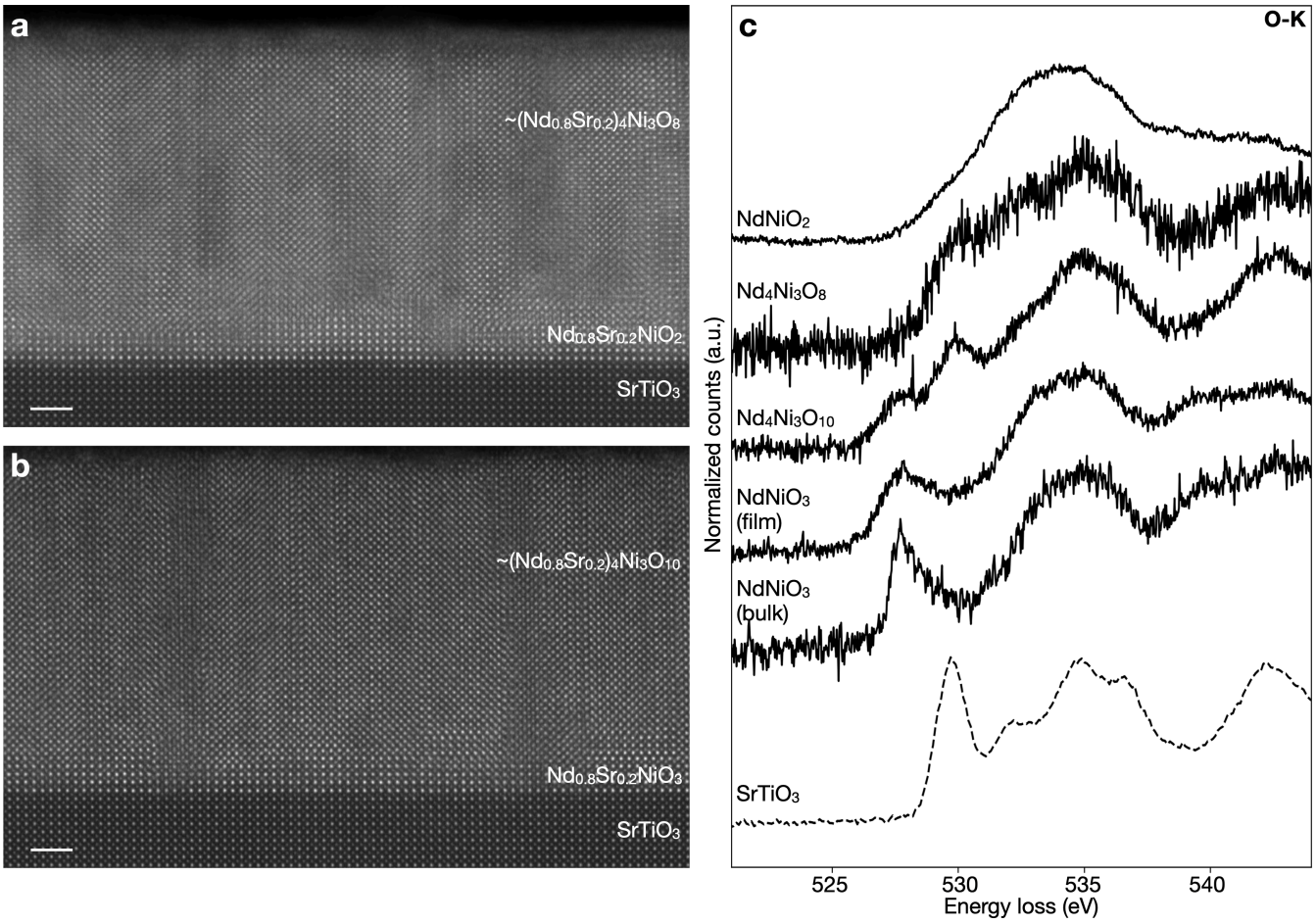


**Fig. S1. Distinct spectral contributions from secondary phases.** Partially optimized synthesis can produce films with significant secondary phases approaching **a**, $(Nd,Sr)_4Ni_3O_8$ and **b**, $(Nd,Sr)_4Ni_3O_{10}$ character, as described in (1). Compared to their pure phase counterparts, $(Nd,Sr)NiO_2$ and $(Nd,Sr)NiO_3$, respectively, these secondary phase regions exhibit markedly different electronic structures evidenced by **c**, the corresponding O-K EELS edges. In optimized film growth (see main text Fig. 1 and (1, 2)), some RP-like defects can still be found, necessitating local spectroscopic measurements to target only the phases of interest. The O-K edge of $SrTiO_3$ is also shown for reference. Scale bars are 2 nm.

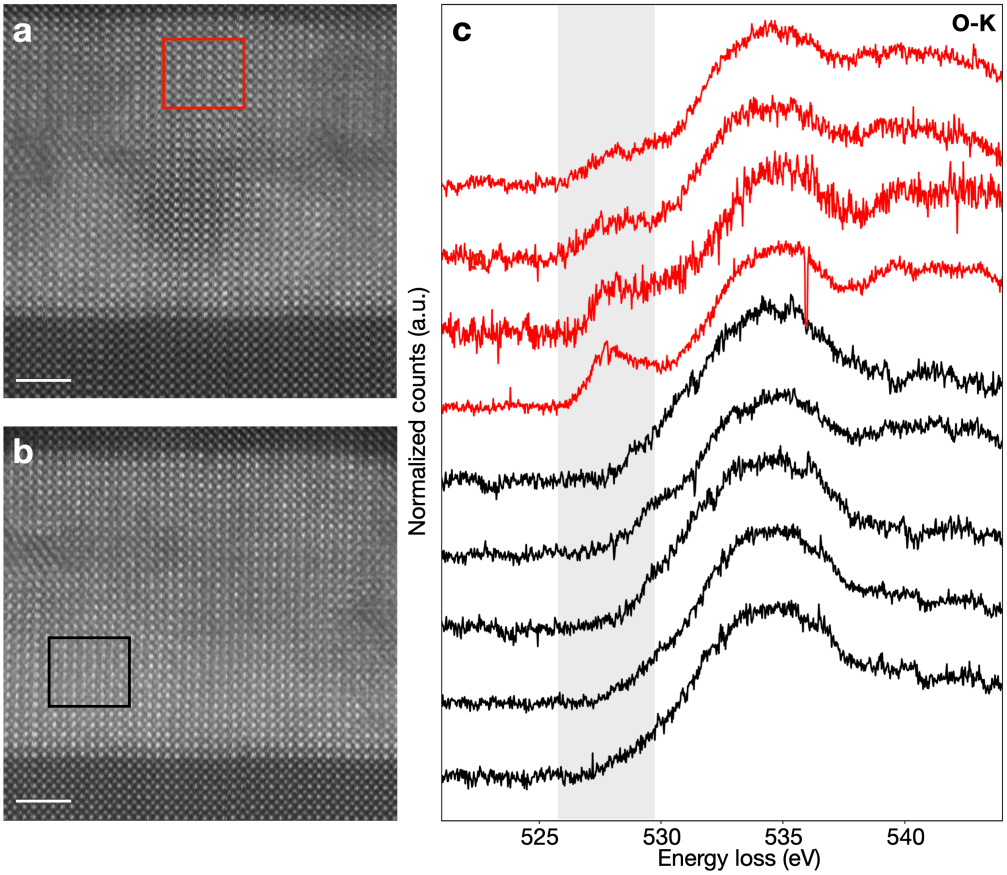


**Fig. S2. Spatial variations of oxygen stoichiometry in a nominal $NdNiO_2$ film. a, b**, HAADF-STEM images of the $NdNiO_2$ film showing areas which appear to be crystallographically clean. **c**, O-K EEL spectra from several different regions throughout the reduced film. Some spectra show signs of oxygen-rich stoichiometry $NdNiO_{2+\delta}$ as judged by the presence of the pre-peak at ∼527 eV discussed in Fig. 1 of the main text. Spectra with edge onset before 527 eV were discounted from further analysis to avoid contributions from such off-stoichiometric regions, here plotted in red. The grey highlighted region is the same as that shown in Fig. 1 of the main text. The red box in **a** shows the EELS acquisition area for one partially-reduced region, while the black box in **b** shows the EELS acquisition area for a fully-reduced region. The two areas are indistinguishable by HAADF-STEM imaging alone; spectroscopic measurements are needed to confirm that measurements are probing the pure infinite-layer phase. Scale bars are 2 nm.

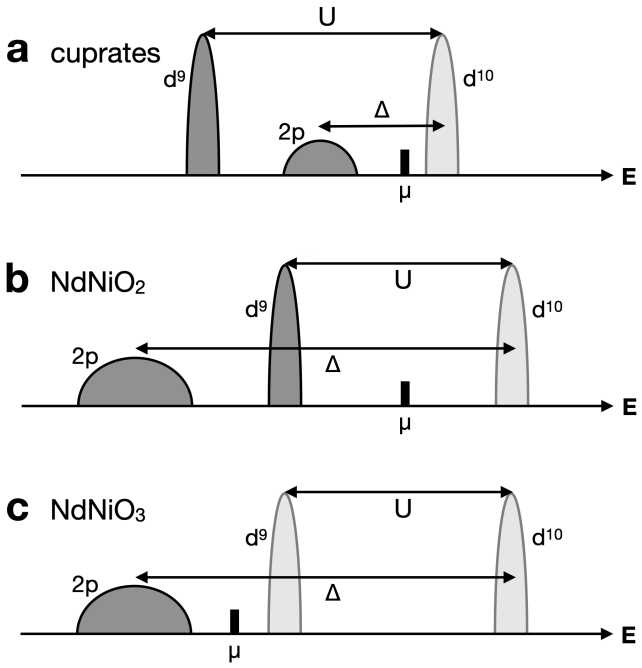


**Fig. S3. Schematic Zaanen-Sawatzky-Allen diagram** illustrating **a**, the charge-transfer cuprates as well as the electronic evolution between **b**, the Mott-Hubbard infinite-layer $NdNiO_2$ and **c**, the perovskite $NdNiO_3$ (5). In this picture, the charge-transfer energy $\Delta$ is greater than the on-site Coulomb interaction $U$, placing $NdNiO_2$ in the Mott-Hubbard regime.

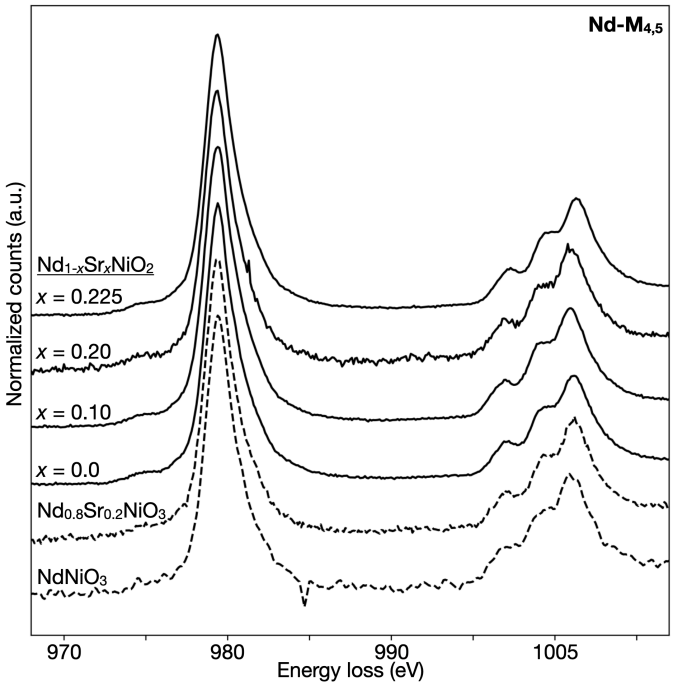


**Fig. S4. Consistent Nd valence in all films.** The Nd-$M_{4,5}$ edge ($4f$ states) shows no apparent change across either O-reduction or hole-doping, consistent with a stable $Nd^{3+}$ formal valence.

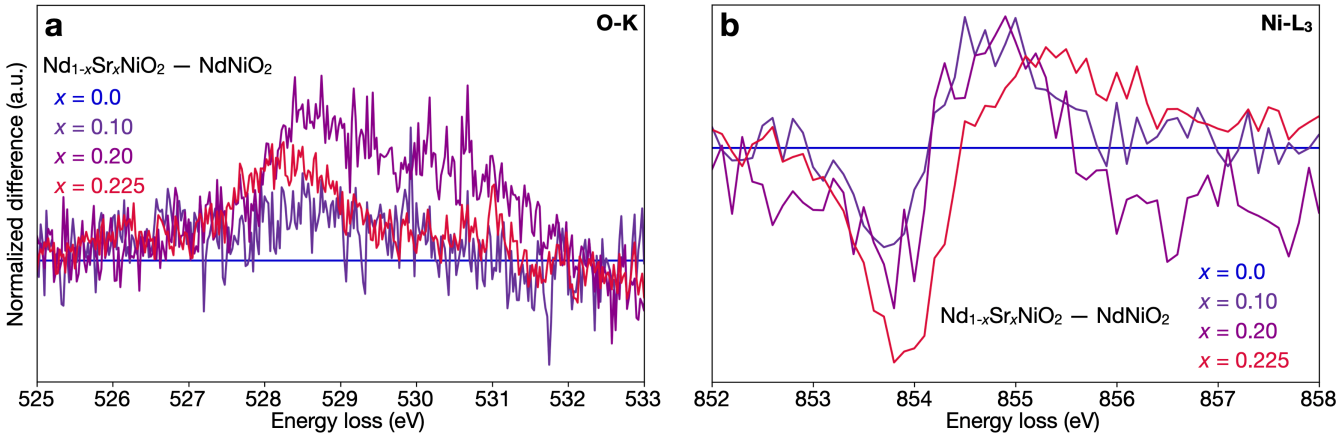


**Fig. S5. Difference spectra of the O-K and Ni-$L_3$ edges for $Nd_{1-x}Sr_xNiO_2$.** Spectral differences across the doped $Nd_{1-x}Sr_xNiO_2$ series are highlighted by subtracting the undoped $NdNiO_2$ spectrum for each edge as a reference. **a**, The increasing strength of the $d^9\underline{L}$ peak at ∼528 eV with hole doping is apparent. The $x$ = 0.2 sample shows additional spectral weight at ∼530 eV, suggesting there may be some contributions to the integrated weight from RP faults similar to Fig. S1. **b**, The Ni-$L_3$ edge shows shifting onset and peak energies with increased hole doping, appearing as dips near ∼854 and peaks near ∼855 eV relative to the undoped film. The $x$ = 0.225 edge in particular also shows a broad tail extending to higher energies.

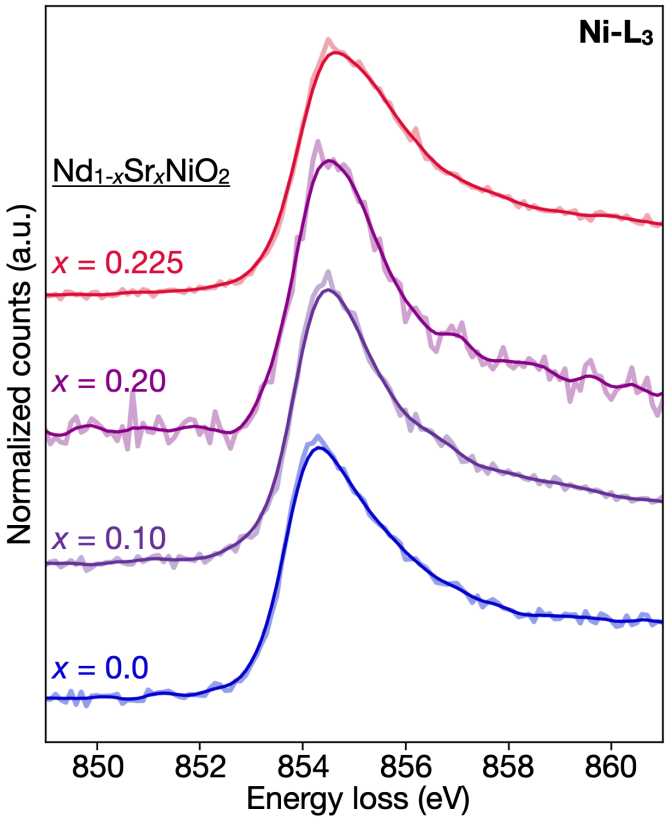


**Fig. S6. Extracting shifts of the Ni-$L_3$ edge in $Nd_{1-x}Sr_xNiO_2$.** Raw Ni-$L_3$ spectra from the $Nd_{1-x}Sr_xNiO_2$ series are normalized by integration from 851-862 eV and smoothed with a weighted average over 5 channels in order to extract the peak positions shown in Fig. 4d of the main text. Raw (light) and smoothed (dark) spectra are plotted together for each doping.

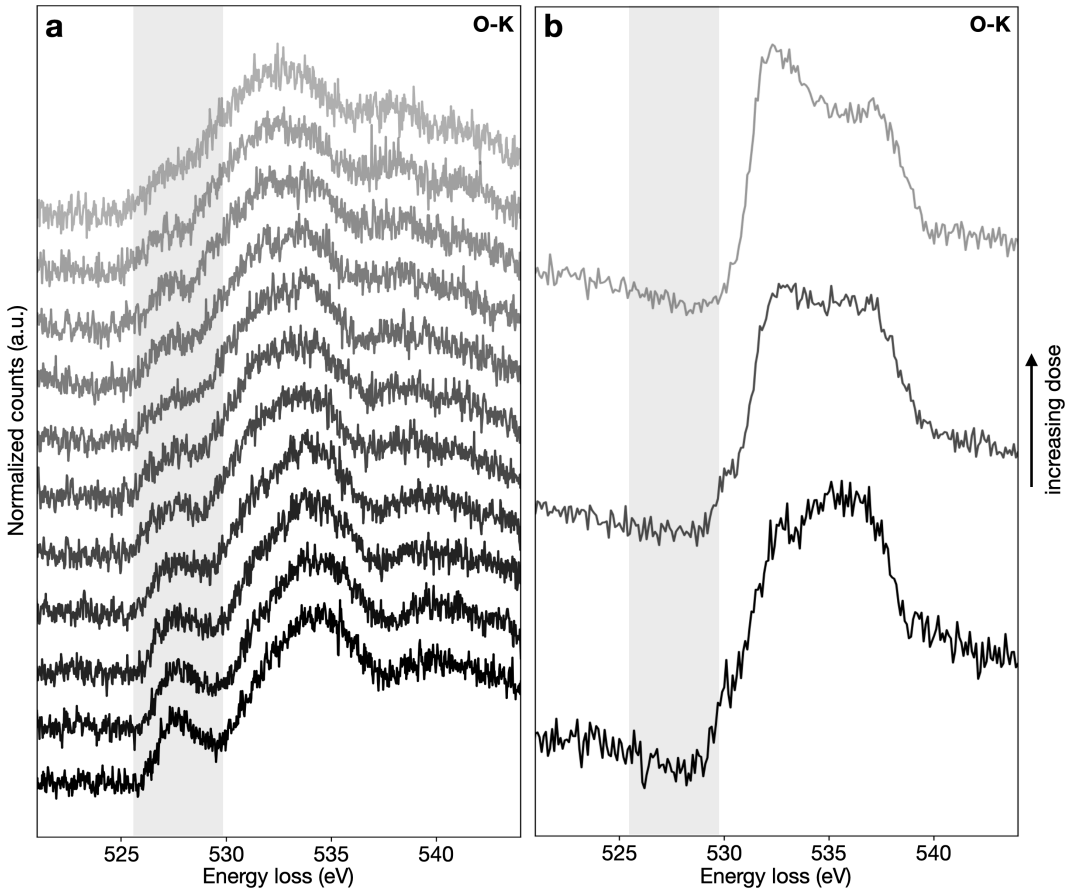


**Fig. S7. Effects of electron-beam induced radiation damage on the O-K edge. a**, The primary effect on $NdNiO_3$ films is an apparent O-reduction under the beam, evolving towards a more $NdNiO_2$-like character evidenced by the decreasing pre-peak in the grey highlighted region (same energies shown in Fig. 1 of the main text). Each spectrum in **a**, corresponds to a subsequent exposure of 200 sec, or $\sim 2 \times 10^7$ $e^-/Å^2$ additional dose. **b**, In $NdNiO_2$ films, a peak at $\sim$532 eV appears and grows with additional exposure. With very high doses ($\sim$2 nA beam current), structural changes can also be observed in HAADF-STEM. At beam currents of $\sim$20 pA, repeated experiments showed no electronic modification in any sample. This beam current was therefore subsequently set as the damage-limited threshold current. Note: O-K spectra are shown here without prior background subtraction.

## References


1. K Lee, et al., Aspects of the Synthesis of Thin Film Superconducting Infinite-Layer Nickelates. *APL Mater.* **8**, 041107 (2020).
2. D Li, et al., Superconducting Dome in $Nd_{1-x}Sr_xNiO_2$ Infinite Layer Films. (2020) arXiv:2003.08506 [cond-mat].
3. MA Hayward, MA Green, MJ Rosseinsky, J Sloan, Sodium Hydride as a Powerful Reducing Agent for Topotactic Oxide Deintercalation: Synthesis and Characterization of the Nickel(I) Oxide $LaNiO_2$. *J. Am. Chem. Soc.* **121**, 8843–8854 (1999).
4. M Hayward, M Rosseinsky, Synthesis of the infinite layer Ni(I) phase $NdNiO_{2+x}$ by low temperature reduction of $NdNiO_3$ with sodium hydride. *Solid State Sci.* **5**, 839–850 (2003).
5. V Bisogni, et al., Ground-state oxygen holes and the metal–insulator transition in the negative charge-transfer rare-earth nickelates. *Nat. Commun.* **7**, 1–8 (2016).
6. A Yasui, et al., Temperature dependence of post-sintered annealing on magnetic properties of intergranular phase in Nd-Fe-B permanent magnet. *J. Appl. Phys.* **117**, 17B313 (2015).